Wax Precipitation from North Sea Crude Oils: I. Crystallization and Dissolution Temperature, and Newtonian and Non-Newtonian Flow Properties

ARTICLE *in* ENERGY & FUELS · NOVEMBER 1991

Impact Factor: 2.79 · DOI: 10.1021/ef00030a019

4 AUTHORS, INCLUDING:

Hans Petter Rønningsen
Statoil ASA
17 PUBLICATIONS **631** CITATIONS
SEE PROFILE

Asger B Hansen
Haldor Topsøe
114 PUBLICATIONS **1,071** CITATIONS
SEE PROFILE

tually be generated during thermal treatment whilst the α,β-isomer can decrease in relative concentration. Such changes would influence $\beta,\beta/\alpha,\beta$-homohopane maturity ratios if they were to occur in source rock kerogen formation or analysis.

Acknowledgment. M.L. acknowledges the award of a University of Melbourne Postgraduate Scholarship and P.W. study leave from the Jianghan Petroleum Institute, Shashi, P. R. China. We thank the referees for helpful comments.

Wax Precipitation from North Sea Crude Oils. 1. Crystallization and Dissolution Temperatures, and Newtonian and Non-Newtonian Flow Properties

Hans Petter Rønningsen* and Brit Bjørndal

STATOIL a.s., Production Laboratories, Forus, N-4001 Stavanger, Norway

Asger Baltzer Hansen and Walther Batsberg Pedersen

Risø National Laboratory, DK-4000 Roskilde, Denmark

Received March 28, 1991. Revised Manuscript Received June 11, 1991

This paper is the first in a series which summarizes experimental work on wax precipitation in North Sea crude oils, leading to an improved thermodynamic model for prediction of wax formation. Seventeen crude oils and condensates were characterized analytically and rheologically with emphasis on properties related to the content of wax. In particular, three different methods for determination of wax precipitation temperature (WPT), namely polarization microscopy, differential scanning calorimetry (DSC), and viscometry, are discussed and results obtained by the three methods are compared. Microscopy invariably gave the highest WPTs and probably the most relevant values for predicting the *onset* of wax deposition on cold surfaces. The WPTs from microscopy were found to depend on factors such as thickness of the sample film and cooling rate. DSC and viscometry are likely to underestimate the onset temperature of initial wax deposition. Activation energies of viscous flow in the Newtonian temperature range (usually above 30–35 °C), calculated by fitting viscosity data to a simple Arrhenius type exponential equation, are presented and found to be closely correlated with type of petroleum fluid. Light condensates had activation energies approaching those of pure *n*-alkanes ($\leq$10 kJ mol^{-1}) while a highly biodegraded heavy oil had an activation energy of nearly 40 kJ mol^{-1}. Finally, compositional analyses of wax precipitated from one of the oils indicated that wax crystallizing just below the WPT was richer in condensed naphthenes and poorer in isoalkanes than wax formed at lower temperatures. Isoalkanes appeared to be the most abundant class at all temperatures.

Introduction

The majority of crude oils and crude oil products contain substantial amounts of petroleum wax. Depending on the kind of oil, the composition of the wax may range from predominantly low molecular weight *n*-alkanes (C_{20}–C_{40}) to high proportions of high molecular weight isoalkanes and cyclic alkanes. The former type of wax is termed paraffin or distillate wax and generally crystallizes as large needles and plates while the latter type is termed microcrystalline or amorphous wax. The precipitation of wax from petroleum fluids may give rise to a variety of problems well-known within the petroleum industry. Numerous papers have addressed problems associated with deposition of wax in pipelines and production equipment[2-7] as well as rheological behavior,[8-16] which is largely dependent on the waxy constituents of the oils. Fundamental issues related to the wax crystallization process,[17-23] crystal morphology,[1,24] and physical properties of petroleum wax[25,26] have been studied in detail. A parameter of

(1) Edwards, R. T. *Ind. Eng. Chem.* **1957**, *49*(4), 750–757.
(2) McClaflin, G. G.; Whitfill, D. L. *SPE Paper* **1983**, No. 12204.
(3) Bott, T. R.; Gudmundsson, J. S. *Inst. Pet. Tech.* **1977**, Tech. Paper IP-77-077.
(4) Bott, T. R.; Gudmundsson, J. S. *Can. J. Chem. Eng.* **1977**, *55*, 381–385.
(5) Agrawal, K. M.; Khan, H. U.; Surianarayanan, M.; Joshi, G. C. *Fuel* **1990**, *69*, 794–796.
(6) Bern, P. A.; Withers, V. R.; Cairns, J. R. *Proc. Eur. Offshore Pet. Conf., London* **1980**, 571–578.
(7) Carnahan, N. F. *J. Pet. Technol.* **1989**, Oct., 1024–1025.
(8) Sifferman, T. R. *J. Pet. Technol.* **1979**, Aug., 1042–1050.
(9) Barry, E. G. *J. Inst. Pet.* **1971**, *57*(554), 74–85.
(10) Agrawal, K. M.; Purohit, R. C.; Surianarayanan, M.; Joshi, G. C.; Krishna, R. *Fuel* **1989**, *68*, 937–939.
(11) Economides, M. J.; Chaney, G. T. *Soc. Pet. Eng. J.* **1983**, June, 408–416.
(12) Seitzer, W. H.; Lovell, P. F. *Proc. Oil Shale Symp., Colorado School of Mines* **1979**, 213–220.
(13) Irani, C. A.; Zajac, J. *J. Pet. Technol.* **1982**, Feb., 289–298.
(14) Perkins, T. K.; Turner, J. B. *J. Pet. Technol.* **1971**, March; 301–308.
(15) Smith, P. B.; Ramsden, R. M. J. *Proc. Eur. Offshore Pet. Conf., London* **1978**, 283–290.
(16) Van Engelen, G. P.; Kaul, C. L.; Vos, B.; Aranha, H. P. *Proc. Offshore Technol. Conf., Houston* **1979**, 1385–1390.
(17) Pudgett, F. W.; Hefley, D. G.; Henriksen, A. *Ind. Eng. Chem.* **1926**, *18*, 832–835.
(18) Koolvoort, E. C. H.; Moser, F. R.; Verver, C. G. *J. Pet. Technol.* **1937**, *23*, 734–745.
(19) Holder, G. A.; Winkler, J. *J. Inst. Pet.* **1965**, *51*(499), 228–252.
(20) Brownawell, D. W.; Hollyday, W. C. *J. Inst. Pet.* **1962**, *48*(463), 209–216.
(21) Ackroyd, G. C.; Cawley, C. M. *J. Inst. Pet.* **1953**, *39*, 82–111.
(22) Affens, W. A.; Hall, J. M.; Holt, S.; Hazlett, R. N. *Fuel* **1984**, *63*, 543–547.
(23) Halter, E.; Kanel, J.; Schruber, D. *Liq. Fuel Technol.* **1985**, *3*(4), 477–487.
(24) Ferris, S. W.; Cowles, H. C. *Ind. Eng. Chem.* **1945**, *37*, 1054–1062.

0887-0624/91/2505-0895$02.50/0

particular practical importance is the wax appearance or precipitation temperature (WPT), traditionally known as the cloud point, at which visible crystallization commences, and below which deposition problems are likely to arise. Furthermore, the *amount* of wax suspended in the hydrocarbon solvent matrix at any given temperature determines the potential for wax deposition, and therefore is essential input to models for prediction of amounts *actually* deposited on cold surfaces, such as pipeline walls.

A number of thermodynamic models for predicting the onset of crystallization as well as equilibrium amounts of wax precipitated, based on either regular solution theory[27,28] or polymer solution theory,[29] have been proposed. The main common deficiency of the models appears to be their inability to predict the wax *amounts* correctly, which rests, at least in part, on the lack of appropriate experimental data for tuning of the models. Therefore, a research program was initiated with the following main objectives: (1) provide experimental wax precipitation data (i.e., precipitation temperatures and amount precipitated as a function of temperature), (2) provide experimental enthalpy data for the liquid–solid transition associated with wax formation, and (3) incorporate the experimental results into an improved thermodynamic model. The present paper is the first in a series of papers summarizing the experimental work and the model development. Two of these, by Hansen et al.[30] and Pedersen et al.,[31] respectively, will describe the differential scanning calorimetry (DSC) and pulsed NMR techniques applied on a series of North Sea crude oils, and one paper by Pedersen et al.[32] will describe in detail the thermodynamic model. The present paper covers the following main topics: (1) chemical and physical characterization of the oils investigated, (2) Newtonian and non-Newtonian rheological properties, (3) the practical use of polarization microscopy, DSC, and viscometry for determination of wax precipitation temperatures, (4) measurement of wax dissolution temperatures, and (5) comparison of results obtained by the different methods for determination of wax crystallization and dissolution temperatures.

Experimental Section

Fluids Investigated. Seventeen North Sea crude oils and condensates from various fields on the Norwegian continental shelf were used in this investigation. They covered a wide range of fluid compositions and physical properties including "normal" paraffinic oils, heavy biodegraded oils, waxy oils, light paraffinic condensates, and waxy condensates. For simplicity, the common designation "oil" will be used for all fluids throughout the text. A brief description of the oils investigated, is given in Table I. Oil no. 13 was in fact a very light condensate, containing a negligible amount of wax. The oils were either stock tank oil stored in Jerry or Salzkottner cans or oil obtained by flashing the pressurized separator oil to ambient conditions. These are referred to as "dead" or stabilized oils, meaning that the content of dissolved gas is only that soluble at ambient pressure and temperature. Some of the oils had been stored for several years and may have been altered by aging processes. This did, however, not affect the general conclusions drawn from the investigation. All cans and bottles were heated to 40 °C and shaken thoroughly before the oil was transferred to gas-tight 1-L stainless steel pretreatment cells. In the cells, they were heated to 80 °C for 2 h (termed *beneficiation*) to erase any memory of previous wax formation, and cooled at a rate of 9 °C/h to 30 or 35 °C. At this temperature, samples for the different analyses were taken from the cell and transferred to the actual instrument. Samples which were not given a thermal pretreatment (i.e., were only heated to 40 °C) are called "as received" oils. The detailed compositions of the oils investigated will be reported together with the thermodynamic model in a separate work.[32] Table II presents some of the essential bulk properties only.

Table I. Brief Description of Oil Samples Used in This Investigation

oil no.	oil characterization
1	biodegraded, aromatic oil
2	paraffinic oil[a]
3	waxy oil
4	waxy condensate
5	waxy oil
6	waxy oil
7	paraffinic oil[a]
8	paraffinic oil[a]
9	waxy oil
10	light, paraffinic oil[a]
11	heavy, biodegraded, naphthenic oil
12	paraffinic condensate[a]
13	very light, paraffinic condensate
14	waxy oil
15	paraffinic oil[a]
16	paraffinic, asphaltenic oil
17	paraffinic oil[a]

[a] This is the kind of oil which sometimes in the text is referred to as "normal" oils.

Microscopy. A drop of thermally pretreated oil (i.e., heated to 80 °C and cooled to 30 or 35 °C) was placed on a glass slide between adhesive tape spacers with a cover glass on top. The sample thickness normally used was approximately 50 μm (one layer of tape). The sample was viewed through a Leitz Laborlux 12 microscope set up for transmitted illumination with crossed Nicols. The microscope was equipped with a 10× magnifying objective with numerical aperture 0.25 and binocular eyepieces with 12.5× magnification. Hence, the total magnification was 125× and the limit of resolution was 1.10 μm. Temperature regulation was provided by a Mettler hot stage coupled to a Mettler FP80 control unit. The sample was heated from abient temperature to 70 °C. After 10 min at 70 °C, no wax could be observed; the sample was then cooled at a rate of 0.5 °C/min (if not otherwise specified) until wax crystals appeared. The wax precipitation temperature is reported as the first temperature where wax crystals could be observed. Normally three parallels were run and averaged. Equivalently, wax dissolution temperatures were measured by heating the same samples from ambient temperature at a rate of 0.5 °C/min until the last crystals disappeared.

Differential Scanning Calorimetry. Crystallization onset temperatures on cooling and the dissolution temperatures on heating were measured by using a Perkin Elmer System 4 microprocessor controlled thermal analyzer interfaced to a Model 3600 data station. Liquid N_2 cooling was applied. The sample compartment was purged with He. Crude oil samples were heated to 80 °C in closed containers and shaken thoroughly before being transferred to tarred sample capsules and weighed. Stainless steel capsules of 75 μL capacity were used for sample and reference. The filled and closed capsules were kept at 80 °C for 10–15 min. Under cooling conditions, the samples were cooled at a rate of 10 °C/min from 80 to −145 °C. In the heating experiments the samples were heated from −145 °C at a rate of 10 °C/min. Five parallel runs were and averaged to improve precision. Blank thermograms were run regularly to compensate for instrument drifting. A series of *n*-alkanes with known melting points and melting enthalpies were used to calibrate the temperature and energy scales (see discussion below). The crystallization onset temperature was determined manually as the onset of the exothermic peak corresponding to the liquid–solid transition. Similarly, the dissolution temperature was taken as the temperature where the solid–liquid exotherm reached the baseline. The ac-

(25) Mazee, W. M. *J. Inst. Pet.* **1958**, *44*(419), 401–405.
(26) Templin, P. R. *Ind. Eng. Chem.* **1956**, *48*, 154–161.
(27) Won, K. W. *Fluid Phase Equilib.* **1989**, *53*, 377–396.
(28) Weingarten, J. S.; Euchner, J. A. *SPE Paper* **1986**, No. 15654.
(29) Hansen, J. H.; Fredenslund, Aa.; Pedersen, K. S.; Rønningsen, H. P. *AIChe J.* **1988**, *34*(12), 1937–1942.
(30) Hansen, A. B.; Pedersen, W. B.; Nielsen, A. B.; Larsen, E.; Rønningsen, H. P. *Energy Fuels*, this issue.
(31) Pedersen, W. B.; Hansen, A. B.; Nielsen, A. B.; Larsen, E.; Rønningsen, H. P. *Energy Fuels*, this issue.
(32) Pedersen, K. S.; Skovborg, P.; Rønningsen, H. P. *Energy Fuels*, this issue.

Table II. Analytical and Rheological Data of Oils Investigated

	oil no.																
	1	2	3	4	5	6	7	8	9	10	11	12	13[a]	14	15	16	17
molecular weight	243.9	210.3	226.1	176.9	262.7	241.0	216.6	205.5	252.9	179.2	311.4	167.2	123.1	233.0	169.1	273.9	229.7
density, kg m^{-3} at																	
15 °C	883.3	842.4	848.7	824.7	865.7	856.3	852.2	840.9	874.9	805.6	933.2	795.5	776.5	861.9	805.2	870.6	857.0
30 °C[b]	873.1	831.6	837.7	813.3			841.2	830.1	864.5	794.1	923.1	783.9	764.7	851.8	798.1	859.9	846.3
40 °C[b]	866.1	824.2	830.3	805.8	847.7	838.5	833.9	822.7	857.4	786.4	916.5	776.1	756.6	844.6	790.5	852.8	839.0
50 °C[b]	859.0	816.8	823.0	798.3	840.5	831.3			850.3	778.6	909.9	768.3	748.5	837.4	782.3	845.7	831.8
60 °C[b]	852.0	809.4	815.6	790.7	833.3	824.0	819.3	807.8	843.2	770.9	903.2	760.4	740.5	830.2	775.0	838.5	824.5
70 °C[b]	844.9	802.0	808.2	783.0	826.1	816.6			836.0	763.0	896.5	752.5	732.4	822.9	767.3	831.3	817.2
80 °C[b]	837.8	794.5	800.8	754.4	818.8	809.3	804.5	792.9	828.8	755.2	889.7	744.6	724.2	815.9	759.5	824.1	809.8
C_{10+},[c] wt %	91.20	82.54	81.61	75.10	90.15	89.12	84.23	80.28	89.79	73.38	97.39	69.32	46.08	86.58	70.56	88.42	85.07
C_{10+}, aromatics,[d] wt %	42.4	29.8	33.8	26.7	28.8	29.0	35.0	35.0	38.6	20.3	46.7	18.6		26.4	22.4	37.8	26.9
total wax,[c,e] wt %	2.2	6.7	14.3	7.5	15.6	14.8	8.0	7.0	14.1	7.0	2.7	6.3	0.0	11.1	4.7	18.3	11.6
purified wax,[c,f] wt %	1.3	5.0	8.1	7.5	10.4	11.3	5.7	5.0	9.7	6.4	0.8	6.2	0.0	7.6	4.4	6.2	8.0
asphaltenes,[g] wt %	0.3	0.2	0.1	0.2	1.2	0.4	0.5	1.3	1.5	0.4	1.5	0.2	0.0	0.6	0.4	4.2	1.4
pour point, °C																	
as received	−26	−12	+16	−8	+26	+25	+2	+8	+15	+4	−22	−16		+18	+4	+6	
minimum[h,i]	<−35	<−20	−8	−8	+16	+13	−25	−30	−6	−22	−32	<−15		+14	<−20	−12	−1
temp cycled to 50 °C[i]	<−35	−20	0	−6	+27	+17	−2	+6	+10	−20	−30	<−15		+16	<−15	−8	+10
kinematic viscosity,[h] cSt																	
80 °C	3.65	2.15	2.96	1.25	3.84	2.86	2.38	2.20	3.73	1.38	11.11	1.11	0.56	2.73	1.19	4.92	2.78
70 °C	4.68	2.50	3.45	1.42	4.60	3.30			4.58	1.49	15.07	1.20	0.62	3.24	1.29	6.04	3.30
60 °C	5.49	2.85	4.14	1.58	5.68	4.06	3.32	3.00	5.55	1.74	21.35	1.36	0.69	3.91	1.50	7.50	3.94
50 °C	7.17	3.57	4.99	1.90	7.07	5.12			7.27	2.08	32.19	1.66	0.74	4.98	1.80	10.29	4.87
40 °C	9.43	4.36	6.57	2.22	9.30	6.61	5.10	5.76	9.69	2.40	50.90	2.02	0.82	6.25	2.13	13.63	6.31
30 °C	13.03	5.48	9.07	2.75					13.8	2.87	87.05	2.42	0.94	8.32	2.49	17.97	9.37
apparent viscosity,[h,j] mPa s																	
30 °C	11.4	4.6	7.6	2.2	19.3	9.0	6.4	4.8	11.9	2.3	80.4	1.9		7.2	2.0	15.5	7.7
20 °C	16.9	8.0	24.9	5.2	155	46.7	11.8	9.8	24.3	5.2	162	3.7		17.1	4.4	34.5	21.2
15 °C	21.7	11.0	44.7	6.1	315	98.5	18.0	14.6	39.4	7.0	235	4.7		54.7	5.5	55.0	36.8
10 °C	28.7	16.2	85.3	10.1	555	180	28.5	21.8	70.4	10.6	347	5.9		119	7.4	93.5	69.7
5 °C	41.1	23.9	169	42.7	900	295	43.0	32.7	143	42.0	550	8.1		218	10.3	160	143
1 °C	56.0	30.6	290	42.2	1270	490			240	55.0	765	16.3		330	13.0	245	240

[a] The kinematic viscosities of this condensate were 1.06 and 1.24 cSt at 20 and 10 °C, respectively. [b] Calculated from measured density at 15 °C using API standard 2540.[35] [c] Weight percent of whole "dead" oil. [d] Preparative fractionation on silica; see ref 36. [e] Acetone precipitation. [f] After removal of polar material from the total wax. [g] Pentane insolubles. [h] Thermally pretreated (or beneficiated) oil. [i] Explained under Pour Point in Experimental Section. [j] At shear rate 100 s^{-1}, cooling rate 12.5 °C/h.

curacy was estimated to be on the order of ±2 °C. For further details about the DSC measurements; see ref 30.

Pulsed NMR. For a detailed description of this method, see ref 31. Briefly, the method utilizes the fact that excited hydrogen nuclei in the solid and liquid phases relax with different time constants. By measuring the time evolution of the decaying NMR signal after excitation, the solid/liquid phase ratio can be obtained.

Viscosity Measurements. Kinematic viscosity of thermally pretreated oils in the Newtonian temperature range was measured by using Ubbelohde glass capillary viscometer tubes with appropriate capillary constants. Measurements were carried out at 10 °C intervals between 30 and 80 °C. The average was taken of three or four parallels at each temperature. The repeatability generally was 0.5–1% relative. The kinematic viscosity (ν, unit centistoke, cSt = 10^{-2} mm^2 s^{-1}) is related to the dynamic viscosity (μ, unit mPa s) as follows:

$$\nu = \mu/\rho \quad (1)$$

where ρ is the density in g/cm^3.

In the non-Newtonian temperature range (i.e., where the viscosity is shear rate dependent), the apparent viscosity was measured as a function of temperature with a Haake RV12 concentric cylinder viscometer equipped with double gap geometry (NV 1, radii ratio 1.02) and M150 or M500 measuring heads. Thermally pretreated samples were loaded into the viscometer at 30 or 35 °C and cooled at selected cooling rates (2.0 or 12.5 °C/h) and rates of shear (30, 100, and 300 s^{-1}) while continuously monitoring the apparent viscosity. The repeatability of the viscosity measurements is a function of temperature as well as oil type, but typically of the order ±10% relative, somewhat higher for the most waxy oils.

Pour Point. Samples were transferred from the pretreatment cell to conventional pour point glass tubes at 30 °C. They were cooled at a rate of 12.0 °C/h from 30 °C and checked for pourability every 2 °C. This procedure slightly deviates from the standard ASTM pour point test.[33] The pour point is the lowest temperature at which a movement of the sample can be observed when the tube is held in a horizontal position for 5 s. The pour point of beneficiated oil, measured by cooling from 80 °C, is termed *minimum pour point* (mpp). After reaching the mpp, the samples were reheated to 50 °C and recooled at the same rate in order to examine their sensitivity to *temperature cycling*. The repeatability of the pour point test generally is about ±2 °C.

Wax Content. The total wax content of the oils was determined by a slightly modified UOP method 46-64, the so-called "acetone precipitation technique" described by Burger et al.[34] About 5 g oil was dissolved in 35 cm^3 of petroleum ether and the wax was precipitated with 110 cm^3 of acetone at −25 °C. After 2 h at −25 °C, the mixture was filtered through a weighed glass fiber filter (Schleicher & Schuell GF 10), and the filter cake was washed with a cold 3:1 mixture of acetone:petroleum ether. The filter was placed in a tarred bottle and the wax still remaining in the filter funnel was washed into the bottle with toluene. The toluene was evaporated at 100 °C and the bottle was reweighed to obtain the percentage of *total wax* in the original oil sample. Next, the wax was extracted from the filter with toluene and the filter removed. Toluene was again evaporated to dryness. The bottle was reweighed and the wax was dissolved in about 10 cm^3

(33) ASTM D97-87. *Annu. Book ASTM Stand.* **1989**, *05.01*.
(34) Burger, E. D.; Perkins, T. K.; Striegler, J. H. *J. Pet. Technol.* **1981**, June, 1075–1086.

of hexane. Finally, coprecipitated polar material and trapped oil were removed by elution with hexane through a short silica column (2 cm SEP-PAK, Millipore). The hexane was evaporated to obtain the percentage of *pure wax*. The repeatability of this method is about ±10% relative.

Asphaltenes. The content of pentane insoluble asphaltenes was determined by precipitation with pentane (1:40 vol:vol) at 5 °C overnight. The oil–pentane mixture was filtered through a 0.45-μm Millipore HAWP cellulose acetate filter, and the precipitate was dried at 50 °C and weighed.

Density and Molecular Weight. A digital frequency density meter (DMA 40 with DMA 602 M measuring cell, Anton Paar KG) was used to measure all densities at 15 °C. Densities at other temperatures were calculated from measured densities at 15 °C using API standard 2540.[35] Number-average molecular weights were determined by freezing point depression of water-saturated benzene solutions by using a petroleum cryoscope (Cryette A Model 5008). For further details of these techniques as well as distillation and hydrocarbon group type analysis, see ref 36.

Results and Discussion

Composition of Oils Investigated. Some essential compositional data and properties of the oils investigated are summarized in Table II. In most of the oils, the C_{10+} fraction made up 80–90 wt % of the stabilized oils. The C_{10+} aromatic hydrocarbon content, determined by preparative fractionation on a silica column,[36] ranged from 20 to about 50 wt %. The biodegraded oils no. 1 and 11, which were more or less depleted in *n*-alkanes, are seen to have the highest aromatic contents (>40%) while the light oils and condensates generally had the lowest. The remaining part of the C_{10+} fractions is predominantly saturated hydrocarbons, and a small fraction, normally less than 5%, is made up from polar material (resins and asphaltenes). Although not large, the polar fraction highly influences the rheological properties of the oils, particularly the waxy ones, by interfering in the wax crystallization process.

With one exception (oil no. 16), the oils contained less than 1.5% (w/w) pentane-insoluble asphaltenes, in most cases lower than 0.5%, and could thus be classified as low-asphaltene oils. This is typical of the majority of North Sea oils. The total wax content of the oils, determined by acetone precipitation at −25 °C, was between 0 and 18 wt %. It is used only as a rough indicator of whether wax deposition problems are likely to be encountered. However, even the oils with a low total wax content (<5%) may give rise to serious wax deposition problems, given the right conditions with respect to temperature, flow regime, etc. The total wax content was found to agree quite well with the content of solid material determined by pulsed NMR at −25 °C.[31] This was interpreted as an indication of the validity of the NMR method.

Wax-Related Properties. The pour point test is, from a rheological point of view, not satisfactory for predicting low-temperature flow properties because it operates under variable and undefined shear stress and therefore cannot be related to any particular practical pumping conditions. In a rheological evaluation it has to be combined with viscosity and yield stress measurements. However, it is useful as a rough indicator of anticipated flow behavior.

It is interesting to notice the large differences between wax precipitation temperatures, as determined by microscopy, and the minimum pour points of the oils. In most cases the pour point was 40–60 °C lower than the WPT, the exceptions being the high-wax oils no. 5, 6, and 14. This may have at least two causes: First, a certain volume of precipitated wax material is needed for an interlocking network to develop. And second, it may be due to the action of natural pour point depressants (PPD), which, like most synthetic PPDs, lower the pour point but do not affect the WPT much (see below). Concerning the first point, Holder and Winkler[19] found that about 2% precipitated wax was sufficient to cause gelling of distillate fuels. One could imagine that somewhat more would be needed for whole crude oils to gel due to their generally higher content of indigenous PPDs; and, in fact, pulsed NMR experiments, the details of which are discussed in a separate paper,[31] seemed to confirm this. Table III lists the minimum pour point temperatures together with the measured amount of solid material present at the same temperature. Experimental uncertainty in the pulsed NMR as well as the pour point measurements taken into account, in almost every case approximately 4 wt % of solid hydrocarbons was present at the gelling temperature when the oils were in their thermally beneficiated conditions. Oil no. 1, and in particular no. 11, behaved differently, probably because these were highly biodegraded oils with a very low total wax content and certainly atypical

Table III. Amount of Wax Precipitated at the Minimum Pour Point

oil no.	min pour point, °C	wt % wax at min pour point[a]
1	−40[b]	6.2
2	−25[c]	4.5
3	−8	3.9
4	−8	4.5
5	+16	5.5
6	+13	4.0
7	−25	4.0
8	−30	5.3
9	−6	3.8
10	−22	3.7
11	−32	>15
12	−30[c]	4.1
13		
14	+14	3.9
15	−30[c]	3.8
16	−12	4.0
17	−1	3.5

[a] Determined by pulsed NMR; see ref 31. [b] Estimated value; the pour point was lower than −35 °C. [c] Estimated value; the pour point was lower than −20 °C.

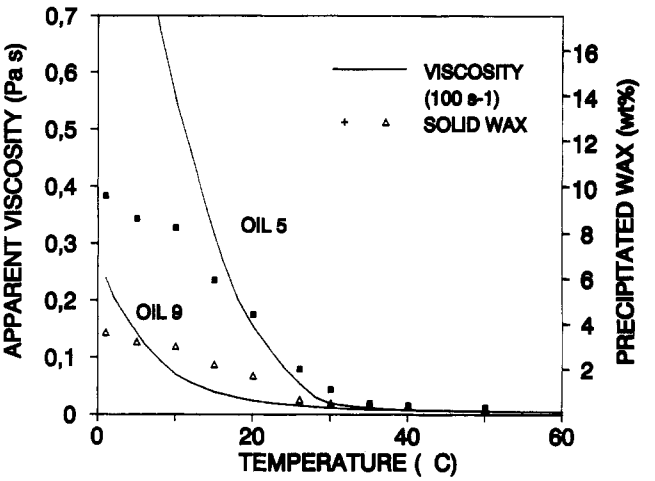

Figure 1. Effect of wax precipitation on the apparent viscosity of two crude oils. The viscometer was cooled at a rate of 12.5 °C/h from 35 °C (oil no. 5) or 30 °C (oil no. 9); shear rate 100 s^{-1}. The content of solid wax as a function of temperature was determined by the pulsed-NMR technique (ref 31).

(35) *Manual of Petroleum Measurement Standards*, 1st ed.; API Standard 2540; American Petroleum Institute: Washington, DC, 1980; Vol. VII, Table 53A.

(36) Rønningsen, H. P.; Skjevrak, I.; Osjord, E. *Energy Fuels* **1989**, *3*, 744–755.

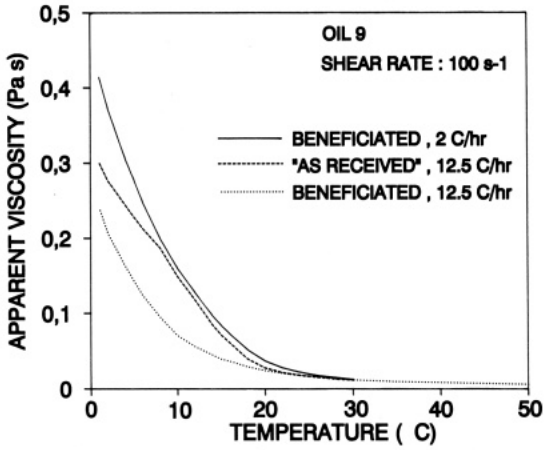

Figure 2. Effect of thermal beneficiation and cooling rate on the apparent viscosity of oil no. 9 at shear rate 100 s^{-1}. Notice the higher viscosity without thermal pretreatment and with slow cooling.

wax compositions with high proportions of isoalkanes and cyclic alkanes.

The connection between wax precipitation and the apparent viscosity of an oil is illustrated in Figure 1. Oils no. 5 and 9 are seen in Table II to have comparable total wax contents, but oil no. 5 has been found by pulsed NMR[31] to contain 2–3 times more solid, suspended wax above 0 °C. This difference is seen to be reasonably well correlated with the viscosities. It can also be noted that in both cases the viscosity started to increase much faster than the solid wax content when this had reached 3–4%, i.e., approximately the amount required the cause gelling.

Effect of Thermal History. Most of the oils, except the condensates no. 4, 10, and 12, were highly sensitive to thermal history; compared to the beneficiated condition, higher viscosities and pour points generally resulted from cycling to an intermediate temperature. As seen in Table II, in some cases the pour point was raised by 30–40 °C after temperature cycling to 50 °C. This may even not be the maximum pour point, as a different reheat temperature could give higher pour point in some cases. The same effect was observed on the viscosity. As a typical example, the effect of thermal beneficiation of oil 9 is shown in Figure 2; with the same cooling rate, the as received oil had about twice as high viscosity as the beneficiated oil at 10 °C (shear rate 100 s^{-1}). This illustrates the strong dependence of crude oil rheology on prior thermal treatment. To obtain meaningful rheological data, deliberate control of the thermal history is crucial.

The dependence on thermal history is believed to be closely associated with the content of indigenous pour point depressants (PPD) found among the polar substances of the oils (resins and asphaltenes), as described by Vos et al.[37] and Moore.[38] Briefly explained, if all the wax is dissolved before cooling commences (i.e., the oil is preheated to 80 °C or higher), the indigenous PPDs are allowed to build into the wax crystals and modify their morphology and surface characteristics and hence their tendency to interact. Furthermore, their action often promotes formation of large crystal aggregates associated with a high fluidity condition. However, when the oil is reheated to an intermediate temperature, the low molecular weight distillate wax is preferentially dissolved while the PPDs are still immobilized. On recooling, the dissolved wax constituents are then allowed to develop an interlocking network, undisturbed by the PPDs, hence the higher pour point. It is worth noticing that even oils containing less than 0.5 wt % asphaltenes, i.e., typical low-asphaltene oils, indeed exhibited pronounced dependence on thermal history.

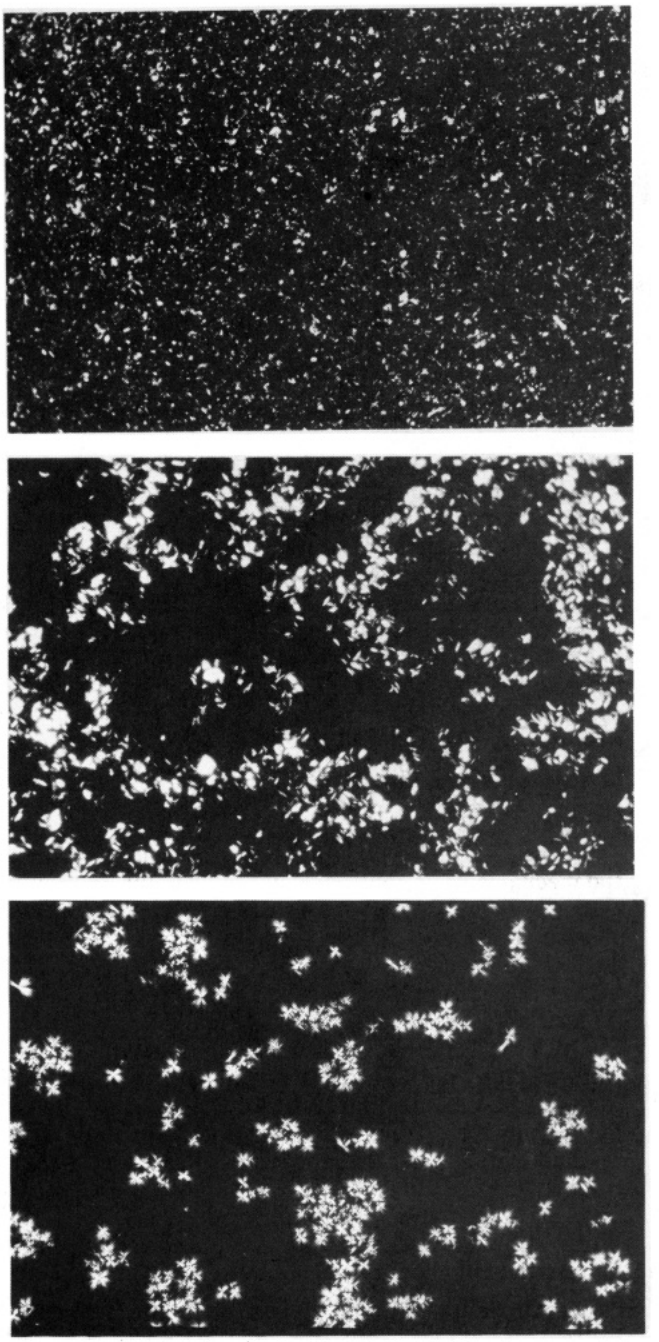

Figure 3. Photomicrographs in polarized light of wax crystals in crude oil no. 5 at room temperature: (a, top) as received oil (i.e., only heated to 40 °C); (b, middle) thermally beneficiated oil (i.e., heated to 80 °C), cooled at a rate of 6 °C/h; (c, bottom) thermally beneficiated oil treated with 200 ppm (w/w) of an EVA type pour point depressant (PPD) added at 55 °C during cooling at a rate of 6 °C/h from 80 to 30 °C. Notice the large crystal aggregates and wax-free regions accompanying the low viscosity and low pour point condition in (b) and the spherulitic crystal structures present in the sample treated with PPD. Scale: The whole width of the photographs covers 700 μm.

The effect of thermal history is also illustrated by the photomicrographs in Figure 3, which clearly show the homogeneous mass of crystals in the as received oil no. 5 (picture a) and the larger aggregates and wax-free regions

(37) Vos, B.; van den Haak, K. *Proc. Indonesian Pet. Assoc., 9th Annu. Conv.* **1980**, May, 501–521.
(38) Moore, R. W.; Beard, L. C., Jr. *Proc. Am. Soc. Testing Mater.* **1932**, *32*, 402–405.

in the thermally beneficiated sample (picture b).

In Figure 2 the strong effect of cooling rate is evident as well. It was generally observed that slow cooling (2 °C/h) gave higher viscosity. This was rather surprising because slow cooling is known to produce larger crystals which have been found to be associated with *low* viscosity.[39-41] It was confirmed by running silicone oil standards that thermal equilibrium in the viscometer–oil system was ensured even with a cooling rate of 15 °C/h. Moreover, pulsed NMR experiments[31] have indicated that nearly the same amount of wax precipitated at a given temperature no matter whether the sample was cooled at a rate of 10 °C/h or was equilibrated for 24 h. It is therefore not clearly understood why slow cooling should give the observed high viscosities.

Effect of Crystal Modifying Additives. The tendency to form crystal aggregates as seen in Figure 3b became even more pronounced and clear in the presence of an effective synthetic PPD or flow improver. A number of commercial additives of the poly(alkyl methacrylate) and ethylene vinyl acetate (EVA) copolymer types have been found to depress the minimum pour point of oil no. 5 far below 0 °C. Effective additives all had in common that they caused the formation of regular, spherulitic crystal aggregates, like those shown in Figure 3c, which were formed in the presence of 200 ppm (w/w) of an EVA copolymer. Similar spherulite structures have been reported by Lovell and Seitzer[12] to be formed in PPD-treated oils as well as neat shale oils.

It is beyond the scope of this paper to go into details on the mechanisms of pour point depression, but the formation of crystal aggregates and eventually spherulitic structures seems in general to accompany a high fluidity condition. Hence, the processes behind the observed effects of thermal beneficiation and PPD treatment probably are similar in nature, although more cultivated in the case of synthetic PPDs.

In the study of PPD additives, no products were found to lower the wax precipitation temperature measured by microscopy significantly. In fact, one of the products (a methacrylate polymer) that gave the largest lowering of the pour point (from +16 to −12 °C in 200 ppm concentration), *raised* the WPT from 40 to about 44–45 °C. Moreover, pulsed NMR measurements with oil no. 5 has indicated that approximately the same amount of wax precipitates at a given temperature with PPD added as without. Hence, the flow-improving effect had to be chiefly due to the organization of needles and plates into weakly interacting spherulitic structures. It should be mentioned that the cross-like appearance of the structures in Figure 3c is an optical artifact.[42] The cross remains stationary on rotation of the stage, indicating that they are actually spherically symmetric with single crystals arranged radially like in bog cotton.

Composition of Precipitated Wax. It is of some relevance for the subsequent modeling work[32] to know which substances are the first to precipitate from solution. Thus, oil no. 4 was equilibrated at three different temperatures (40, 23, and 6 °C) and the precipitated wax obtained by filtration. In this transparent, yellow condensate with WPT about 48 °C (microscopy), solid wax was clearly visible at all these temperatures. Oil no. 4 was chosen for these experiments because waxes filtered from the more viscous, black oils were likely to contain much more trapped liquid. It could be noticed that the amount of wax filtrated at 6 °C was approximately the same as the amount determined by pulsed NMR to be present at the pour point, −8 °C (see Table III). However, it was indicated by the pulsed NMR data that the amount of solid material leveled off in the temperature interval from about +5 to −20 °C and hence was nearly the same at 6 °C as at −8 °C.[31]

Table IV. Composition of Wax Filtered from Oil No. 4 at Different Temperatures As Determined by HTGC/MS[a]

	wax filtered at		
	40 °C	23 °C	6 °C
wt % of oil	0.2	1.5	4.5
wt % between C_{16} and C_{40}[b]	50	67	73
	normalized vol % of material between C_{16} and C_{40}		
n-alkanes	20.5	26.4	20.3
isoalkanes	41.9	49.3	60.4
mononaphthenes	13.3	11.7	13.8
dinaphthenes	14.6	9.9	3.8
trinaphthenes	3.8	0.8	1.0
tetranaphthenes	1.9	0.7	0.5
pentanaphthenes	0.0	0.0	0.0
hexanaphthenes	0.0	0.0	0.1
monoaromatics	4.0	1.2	0.0

[a] Gives the composition in the carbon number range C_{16}–C_{40}. [b] Ratio C_{16}–C_{40} area/total area.

The filtered waxes were analyzed by high-temperature gas chromatography/mass spectrometry (HTGC/MS). This method was based on ASTM D2786[43] and gave the distribution of saturate hydrocarbon classes, limited upwards to carbon number C_{40} and downwards to C_{16}. The compositions of the waxes are summarized in Table IV.

Two factors made the compositional data somewhat uncertain: First, because the waxes contained quite large C_{40+} fractions, the overall composition may differ somewhat from the composition between C_{16} and C_{40}; and second, the filtered waxes inevitably contained some trapped oil which added to the wax compositions. Therefore, the compositions given in Table IV have to be used with some care. Some trends which likely reflected the real differences reasonably well, could, however, be extracted: The isoalkane class was dominating in the filtered wax and the amount relative to the *n*-alkanes was getting larger with decreasing temperature. Furthermore, there was a considerable contribution from cyclic alkanes, particularly mono- and dicyclic, probably with various alkyl groups substituted. Compared to the other samples, the wax filtered at the highest temperature contained more polycyclic naphthenes and some monoaromatics. Because of the large fraction of C_{40+} material (50%) in this wax, the overall composition may, however, differ considerably from the composition between C_{16} and C_{40}. Also, the *n*-alkane distribution was found to be shifted toward lower carbon number with decreasing temperature. While the peak of the distribution was around C_{50} in the 40 °C wax, it was around C_{42} and C_{33} in the 23 and 6 °C waxes, respectively.

As mentioned above, because of the limited carbon number range covered by the GC/MS method, it is not possible to draw safe conclusions about which substances dominate the initial crystallization. The results indicated, however, that the relative abundance of substituted polycyclic naphthenes was getting larger near the crystalli-

(39) Hutton, J. F. *J. Inst. Pet.* **1959**, *45*(425), 123–129.
(40) Russell, R. J.; Chapman, E. D. *J. Inst. Pet.* **1971**, *57*(554), 117–128.
(41) Tuttle, R. N. *J. Pet. Technol.* **1983**, June, 1192–1196.
(42) Lovell, P. F.; Seitzer, W. H. *Prepr. Pap.—Am. Chem. Soc., Div. Fuel Chem.* **1978**, *23*(4), 38–45.
(43) ASTM D2786-86. *Annu. Book ASTM Stand.* **1989**, *05.02*.

zation temperature, while the isoalkane class was still most abundant. It should be emphasized that these trends might be different for other oils. The overall chemical composition of petroleum waxes has been discussed by several authors.[21,25,44]

Methods for Determination of Wax Crystallization Temperature 1. Standard Methods. Two standard methods exist for determination of onset temperature of wax crystallization in petroleum fluids: (1) ASTM D2500 (IP 219)[45] for determination of cloud point of petroleum oils and (2) ASTM D3117[46] for determination of "wax appearance point" of distillate fuels. Both methods apply to liquids which are transparent in layers about 30 mm in thickness and hence come short when most black oils are to be examined. In the following paragraphs the characteristics of three fundamentally different methods for detecting the onset of wax crystallization in black (as well as transparent) oils are discussed. Furthermore, results obtained by each method for the 17 oils investigated, are compared.

2. Polarization Microscopy. The utilization of polarization microscopy for the study of wax crystallization is based on the fact that all crystalline materials with noncubic geometry are optically anisotropic, meaning that the crystals rotate the plane of polarization of transmitted, polarized light. Hence, by crossing two Nicol prisms on opposite sides of the sample, all light is initially blocked. On cooling, the crystallizing material appears as spots against a black background. Polarization microscopy has had widespread use for the study of crystallization conditions[19,22] as well as the influence of inherent substances[18,38] and additives[21,47,48] on wax crystallization.

Concerning the practical use of polarization microscopy for determination of WPT, there are several things to be aware of. First, there is, of course, a certain detection limit with respect to crystal size which depends primarily on the total magnification of the microscope. It may be lowered by increasing the magnification, but 125× total magnification as obtained with a 10× magnifying objective and 12.5× magnifying eyepieces has been found to be a satisfactory compromise between image brightness and magnification. Particles larger than about 0.5 μm are then visible. Sometimes, however, "noise" produced by dust particles may be difficult to discern from tiny crystals. Although probably of minor practical importance, tiny wax crystals could be present even before anything is seen in the microscope. On a volume basis, the detection limit is likely to be somewhat lower than for the alternative DSC and viscometry techniques to be discussed below.

In a visual technique like this, a certain element of operator dependence is inevitably involved. Hence, though measurements made by one operator normally are repeatable within about 1 °C, results obtained by different operators typically agree within 1.5–2 °C. These figures are also to some extent oil-dependent. The crystals are easier to detect and the repeatability is hence better with some oils (often the waxy ones) than others. Tiny crystals which precipitate from oils poor in *n*-alkanes may be rather difficult to detect accurately. Moreover, it has been experienced that the time taken for a certain number of wax crystals to develop may vary considerably. If a lot of crystals develop soon after the first crystals appear, which often occurs in waxy oils, it is much easier to establish the WPT accurately.

Table V. Effect of Film Thickness and Cooling Rate on Observed WPT[a] of Two Crude Oils (Each in Duplicate) with Polarization Microscopy

	oil no. 15[b]		oil no. 6[c]	
cooling rate 0.5 °C/min				
no spacer[d]	40.5	40.5	41.5	42.0
50 μm[e]	35.0	34.5	39.0	38.5
100 μm[f]	32.0	32.0	38.0	38.5
150 μm[g]	31.5	32.0	39.0	39.5
film thickness 50 μm				
0.1 °C/min	39.0	38.0	41.0	41.5
0.2 °C/min	38.0	38.5	41.5	41.5
0.5 °C/min	35.0	34.5	39.0	38.5

[a] Wax precipitation temperature. [b] A light, paraffinic, moderately waxy oil. [c] Waxy oil. [d] Cover glass directly on sample. Sample thickness dependent on the viscosity of the oil, but probably of the order 10 μm. [e] One layer of adhesive tape spacer; thickness not measured exactly. [f] Two layers of tape. [g] Three layers of tape.

In any crystallization process, one has to be aware of the effect of cooling rate. In the limit of zero cooling rate, the system will approach thermal equilibrium. An increased cooling rate will drive the system out of equilibrium, thus allowing for underestimation of the crystallization temperature. However, to operate close to equilibrium conditions would require exceedingly long experiments. Therefore, we had to quantify the effect of cooling rate in order to find an appropriate cooling rate for practical purposes. Table V summarizes the effect of cooling rate for two oils. In both cases there was a certain effect. Increasing the rate from 0.1 to 0.5 °C/min lowered the observed WPT by about 4 and 3 °C for oils no. 15 and 6, respectively. But 0.5 °C/min has been chosen as the standard cooling rate in practice, although a slower rate would be slightly more accurate.

Another factor which has been found to influence the measured WPTs is the thickness of the oil film. When a cover glass is applied directly on the sample, it is squeezed out to an unpredictable thickness determined essentially by the viscosity of the oil. For oils no. 15 and 6, WPTs measured this way were 40.6 and 41.5 °C, respectively. Table V shows the effect of increasing the sample thickness by inserting adhesive tape spacers between the object glass and the cover glass. The thickness of one layer was estimated to be about 50 μm. It is seen that increasing the sample thickness lowered the observed WPT. Going from no spacer (probably about 10 μm) to 50 and 100 μm lowered the WPT from 40.6 to 35.0 and 31.9 °C, respectively, for oil no. 15 and from 41.5 to 39.0 and 38.0 °C for oil no. 6. Hence, the first spacer inserted caused most of the lowering and the magnitude of the lowering appeared to depend somewhat on the kind of oil. The effect of increasing film thickness to 50 μm was further examined for a series of oils and found to be a general effect, although of different magnitude for different oils. Among 10 oils examined, the WPT lowering induced by increased film thickness amounted to from 1 to 9 °C and about 5 °C on average. The reasons for the higher WPTs observed in the thin-film samples probably were somehow associated with interactions with the glass surface. Without spacer inserted, the thickness of the sample layer is in fact not much larger than normal crystal sizes. In larger volumes, however, crystallization is believed to take place in a more "natural" and less restricted way. Similar observations, although not quantified, have been reported in the literature by Edwards[1] and Holder and Winkler,[48] who found it advantageous to let the wax crystallization take place in bulk volumes. An additional argument for using a

(44) Branthaver, J. F.; Thomas, K. P.; Dorrence, S. M.; Heppner, R. A.; Ryan, M. J. *Liq. Fuels Technol.* **1983**, *1*(2), 127–146.
(45) ASTM D2500-88. *Annu. Book ASTM Stand.* **1989**, *05.02*.
(46) ASTM D3117-87. *Annu. Book ASTM Stand.* **1989**, *05.02*.
(47) Zimmer, J. C.; Davis, G. H. B.; Frohlich, P. K. *Penn. State Collect. Bull.* **1933**, *12*, 57–63.
(48) Holder, G. A.; Winkler, J. *Nature* **1965**, 719–721.

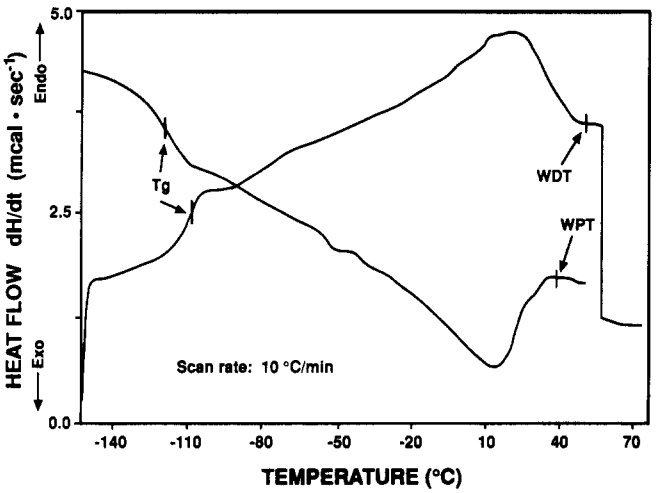

Figure 4. Crystallization exotherm and melting/dissolution endotherm of oil no. 5 obtained by differential scanning calorimetry at scan rate 10 °C/min. The oil was cooled from 80 to −145 °C and then reheated to 80 °C. T_g = glass transition temperature, WPT = wax precipitation temperature (cloud point), and WDT = wax dissolution temperature.

spacer was that the crystals generally were easier to detect and the repeatability was better. In conclusion, use of a spacer, i.e., about 50 μm film thickness, combined with 0.5 °C/min cooling rate, has been adopted as standard conditions.

3. Differential Scanning Calorimetry (DSC). DSC has been widely used for determination of crystallization onset temperatures in petroleum products.[49-52] The method is based on detection of the latent heat of fusion released during crystallization, giving rise to an exothermic peak in the thermogram on cooling, as illustrated in Figure 4 (oil no. 5). The corresponding wax dissolution endotherm is shown as well. It can be noted that the wax crystallization/dissolution processes occur over a temperature range about 140 °C wide, reflecting the very broad carbon number distribution of petroleum wax. The details of the DSC measurements are given elsewhere,[30] but some points essential for the temperature determinations have to be discussed here.

Of crucial importance for correct determination of crystallization (WPT) and dissolution temperatures (WDT) is the calibration of the temperature scale. The instrument was initially calibrated with an indium standard with melting point 156.4 °C. However, as the thermal events associated with wax crystallization occurred at much lower temperatures (<50 °C), potential temperature offset had to be assessed by mean of *n*-alkane standards (>99% purity). The observed melting point, determined as the intersection of the processing baseline and the tangent to the leading edge of the melting endotherm at a scan rate of +10 °C/min, was on average 6 °C higher than the actual melting points. The error introduced by not correcting the slope of the tangent for impurities in the *n*-alkane standards was found to be marginal, in the case of *n*-C_{18} (melting point 28.24 °C) less than −1 °C.

The +6 °C error was initially suspected to include a certain temperature lag due to the heating rate in addition to the actual instrument offset. As in the microscopic measurements, slow heating/cooling scans would be desirable from an equilibrium point of view. And the work by Faust[51] on waxes and petrolatum indicated a slight temperature lag due to nonequilibrium at scan rate 10 °C/min. However, small sample volumes and the fact that the signal is the *time derivative* of the enthalpy change generally restricted the use of scan rates lower than 10 °C/min. The *n*-C_{18} standard was therefore used to examine the influence of scan rates in the range 2.5–10 °C/min on observed temperatures. It turned out that the heating/cooling rate did not have a significant effect on the observed melting and crystallization temperatures,[31] which was in agreement with observations made by Heino[52] for middle distillates. This, in turn, implied that the temperature lag due to instrument offset alone, was +6 °C. Consequently, WPTs and WDTs reported in this paper were obtained by correcting the raw data by −6 °C.

A source of uncertainty in the reported temperatures was the baseline determination. It was sometimes rather difficult to decide exactly where to draw the baseline in the high-temperature region, and consequently to establish the exact onset temperature (i.e., where the curve first deviated from the baseline). Drawing of the baseline also inevitably introduced some operator dependence in the procedure.

In conclusion, the overall accuracy of the reported WPTs and WDTs was estimated to be on the order of ±2 °C. Replicate measurements generally agreed within ±1 °C.

4. Viscometry. The potential of viscosity measurements as a method for determining the onset temperature of wax crystallization lies in the gradual change of rheological properties of an oil that occurs as wax precipitates. Above the wax precipitation temperature, almost any crude oil, with exception of extremely asphaltene-rich oils, is a Newtonian fluid; i.e., the viscosity is a single-valued function of temperature in laminar flow. The temperature dependence in the Newtonian range is most often adequately expressed by a simple exponential Arrhenius or Guzman–Andrade[53] type equation

$$\mu = Ae^{E_a/RT} \tag{2}$$

where μ is the Newtonian dynamic viscosity, E_a is viewed as the activation energy of viscous flow, A is a constant largely dependent on the entropy of activation of flow, R is the universal gas constant, and T is the absolute temperature. A and E_a can generally be considered constant over limited temperature ranges.[54] Below the non-Newtonian temperature limit, μ has to be replaced by the apparent or shear rate dependent viscosity η. The constant A and E_a will in general be functions of shear stress or rate of shear.

Utilizing the fact that the crude oil viscosity obeys eq 2 until wax starts to precipitate, a wax precipitation temperature can be estimated in two ways:

1. The first makes use of the linear relationship between ln μ and $1/T$. The slope of a plot of ln μ against $1/T$ is equal to E_a/R. As wax becomes suspended in the oil, E_a is likely to increase, resulting in a larger slope. This is illustrated for oil no. 5 in Figure 5a. The WPT is identified as the temperature corresponding to the break in the curve.

2. The second approach is first to fit the Newtonian viscosities over a sufficiently broad temperature range, at least 40 °C, to the Arrhenius equation. The lowest temperature included in the fit should be one where the viscosity still lies on a straight line in a semilog plot. The viscosity–temperature curve predicted by the Arrhenius

(49) Claudy, P.; Letoffe, J.-M.; Chague, B.; Orrit, J. *Fuel* **1988**, *67*, 58–61.
(50) Noel, F. *Thermochim. Acta* **1972**, *4*, 377–392.
(51) Faust, H. R. *Thermochim. Acta* **1978**, *26*, 383–398.
(52) Heino, E.-L. *Thermochim. Acta* **1987**, *114*, 125–130.
(53) Andrade, E. N. da C. *Nature* **1930**, *125*, 309–310.
(54) Bestul, A. B.; Belcher, H. V. *J. Appl. Phys.* **1953**, *24*(6), 696–702.

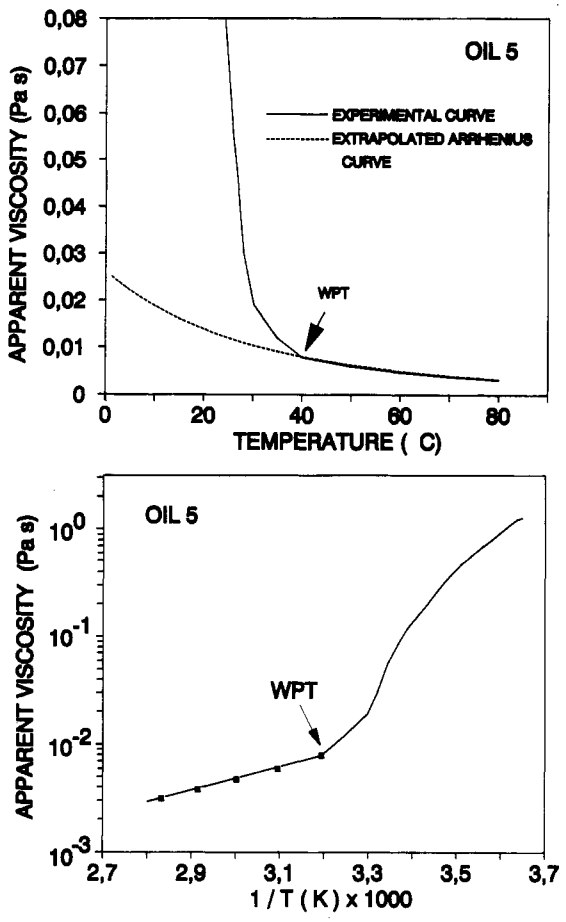

Figure 5. Determination of wax precipitation temperature from viscosity–temperature curve of oil no. 5; cooling rate 12.5 °C/h; shear rate 100 s^{-1}. (a, top) Linear viscosity–temperature plot; WPT identified as the first temperature where the experimental curve deviates from the extrapolated Arrhenius curve. (b, bottom) Arrhenius plot; WPT identified as the temperature where the slope of the curve starts to deviate from linear.

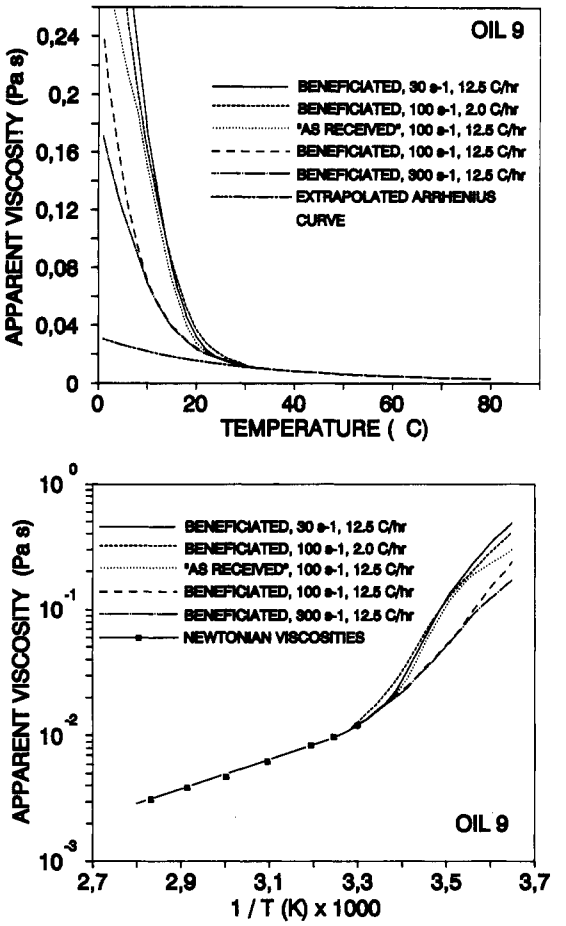

Figure 6. Effect of thermal beneficiation, shear rate and cooling rate on the apparent viscosity of oil 9. (a, top) Linear plot, (b, bottom) Arrhenius plot. Notice that the curves converge toward a single point. The viscometric WPTs were thus essentially unaffected by the condition of the oil.

equation is extrapolated to low temperatures and plotted in a linear graph together with the experimental curve. The WPT is identified as the point where the experimental and predicted "Newtonian" curves separate. This is illustrated for oil no. 5 in Figure 5b.

The choice of approach is largely a matter of convenience, as they are fully equivalent. The results presented in this work were obtained by the second approach. Because the accuracy of the determination will largely depend on how distinct the deviation from the Arrhenius curve is, it is desirable not to use too high shear rate, since the oils are generally shear-thinning. Because the cooling rate and the thermal history has been seen to highly influence the apparent viscosity, these factors had to be assessed as well. A typical example of the effects is illustrated in Figure 6. Neither cooling rate nor thermal history, i.e., whether the oil was thermally beneficiated or not, was found to influence the WPT significantly, meaning that the effects were within the repeatability of the method, which was approximately ±1.5 °C. The results presented here refer to thermally beneficiated oils which were cooled at a rate of 12.5 °C/h at a shear rate of 100 s^{-1}.

The apparent viscosity vs temperature curves in Figures 5–7 were obtained by continuously monitoring the shear stress while cooling the oil at the specified constant shear rate. Somewhat different viscosity values probably would have been obtained if the sample had been cooled statically (i.e., without shear) between subsequent measurements at progressively lower temperatures with, say, 5 or 10 °C intervals. However, the onset of deviation from the Arrhenius curve would probably not have been shifted significantly.

Table VI. Wax Precipitation Temperatures (WPT) Determined by Microscopy, Differential Scanning Calorimetry (DSC), and Viscometry

	WPT from		
oil no.	microscopy[a]	DSC[b]	viscosity[c]
1	30.5	11.0	23
2	38.5	17.0	28
3	41.0	33.5	35
4	48.0	32.5	31
5	39.5	39.5	40
6	39.0	39.5	39
7	34.5	32.0	28
8	38.0	32.0	31
9	35.5	31.5	34
10	41.0	31.5	29
11	22.0	nd[d]	32
12	32.0	25.5	30
13	<5	-26.0	<10
14	33.5	23.0	30
15	35.0	20.5	30
16	37.0	34.0	30
17	39.0	24.0	34

[a] Cooling rate 0.5 °C/min. [b] Cooling rate 10 °C/min. [c] Cooling rate 12.5 °C/h; shear rate 100 s^{-1}. [d] No distinct onset of wax precipitation could be detected.

Comparison of WPTs Obtained by Microscopy, DSC, and Viscometry. Table VI summarizes the WPTs of the oils investigated, obtained by polarization micros-

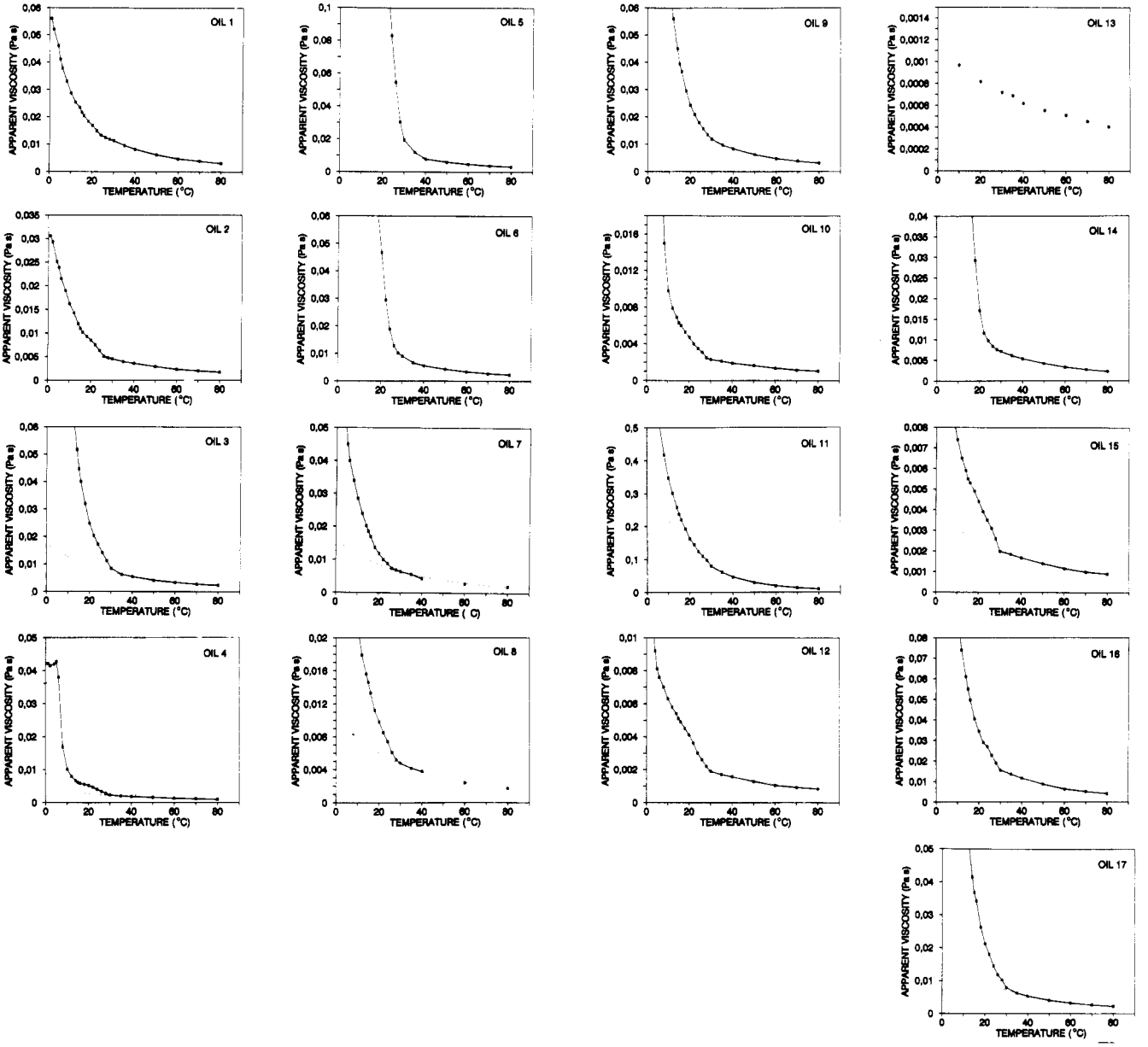

Figure 7. Viscosity–temperature curves of the oils investigated. Cooling rate in the non-Newtonian temperature range was 12.5 °C/h; shear rate was 100 s^{-1}. The WPTs determined from these curves are summarized in Table VII.

copy, differential scanning calorimetry, and viscometry. Due to very small thermal effects, the DSC results for oils no. 1 and 11 were rather uncertain. In oil no. 13, no crystallization was observed above 0 °C by means of microscopy and viscometry. DSC, however, revealed a distinct *n*-alkane exotherm starting at −26 °C.[30] The crystallization temperatures from microscopy were typically between about 35 and 40 °C. The highest value measured was 48 °C for the waxy condensate no. 4. Such a high WPT is unusual for condensates. However, the same has been observed for other similar North Sea condensates. These fluids appear to have in common a certain content (0.2% for oil no. 4) of gray/white pentane-insoluble material that obviously is not regular asphaltenes. Some preliminary pyrolysis–GC analyses have indicated some kind of high molecular weight amorphous wax. It should be noticed that the oils with the highest wax contents (no. 5 and 6) had not particularly high WPTs, only about 39.5 °C. In these oils, however, more extensive wax crystallization was generally observed just below the WPT.

It is evident that the microscopic method for the majority of the oils gave the highest WPTs. The reason for this general trend is likely to be a matter of sensitivity; the DSC and viscometric methods both require a certain amount of solid material for a thermal or viscosity effect to be detected. However, although the microscopic method was seen in some cases to give values more than 10 °C higher than DSC and viscometry, in some cases the difference more or less vanished (or was at least within the experimental error limits). This could somehow be related to the compositional differences between the oils and their wax fractions, for instance, that *n*-alkane crystals were easier to detect in polarized light than crystals made up mainly from branched and cyclic alkanes. More likely, however, it was related to the rate of crystal growth with decreasing temperature. The pulsed NMR measurements[31] indicated that the oils having the lowest DSC onset temperatures (no. 2, 12, 14, 15, and 17) also displayed a nearly constant and low content of solid material above that temperature. It appeared that a threshold value of about 0.3–0.4 wt % had to be exceeded for a thermal effect to be detected.

Figure 7 shows the viscosity–temperature curve at shear rate 100 s^{-1} for each oil together with the extrapolated

Arrhenius curves. With the exception of the biodegraded oils no. 1 and 11, the crystallization temperatures obtained from the viscosity measurements, were, like the DSC values, in most cases around 30 °C. The percentage of solid material present in the oils at the viscometric WPT was about 0.3–0.4% in most cases. Although the NMR data were rather uncertain at this low level, this seemed to be approximately the amount required to induce deviation from the Arrhenius type of temperature dependence as well as a thermal effect in the DSC measurements. Roughly then, the sensitivity in terms of weight percent of solid material required to produce a measurable effect appeared to be about 0.1% for the microscopic method and 0.3–0.4% for the DSC and viscometric methods, respectively.

As opposed to the microscopy and DSC methods, which operate under static conditions, the viscometric method is dynamic. The reasonable agreement between DSC and viscometry in most cases indicated that the use of static methods to predict onset of precipitation under dynamic conditions can be justified, at least as long as the flow is laminar.

Transition from Newtonian to non-Newtonian behavior, identified by a nonlinear shear stress–shear rate dependence, has in most cases been found to occur at least 5–10 °C *below* the viscometric WPT. As an example, oils no. 5 and 6 (WPT 39–40 °C) showed no sign of non-Newtonian behavior above 33–34 °C. The most extreme example is oil no. 11, which behaved strictly Newtonian even at 5 °C, but still showed deviation from the Newtonian Arrhenius curve already at about 30 °C. One possible explanation is that the parameters A and E_a in the Arrhenius equation are slightly temperature dependent even in the Newtonian temperature range and that a slightly steeper curve should be used below, say, 30 or 40 °C. That would in the case of oils no. 5 and 6 give a WPT somewhat lower and closer to the temperature where the viscosity curve starts to increase rapidly, i.e., around 30 °C. For oil no. 11, only a slight adjustment of the extrapolated Arrhenius curve would make the two curves coincide.

In view of the different WPT estimates given in Table VI, the following question arises: Which are the "correct" ones? Despite the somewhat disturbing effect of film thickness discussed above, the microscopic WPTs are considered to be the most relevant values for predicting initial *onset* of wax deposition in flow lines and production equipment. The DSC and viscometric values may be more relevant for predicting onset of *severe* wax deposition problems; although solid dispersed wax obviously is present at the microscopic WPT, the amount might be too low to create problems of any practical significance until a somewhat lower temperature is reached. One should, however, recall that the microscopic WPTs already were slightly underestimated (about 3 °C) compared to equilibrium values due to nonequilibrium experimental conditions (cooling rate). It is worth noticing that, for the most waxy oils (no. 5, 6, and 9), all three methods gave nearly identical results (39–40 °C).

Two factors that might be of importance in many real transport situations have not been considered in this work: The first is the effect of turbulent flow; although laminar flow, as discussed above, did not appear to raise WPT significantly, one could anticipate that nucleation and crystal growth occurred easier under turbulent conditions. At least, turbulence is likely to influence the degree of *deposition*. The second factor not considered here is the effect of solution gas present in unstabilized or partly stabilized reservoir oils. Weingarten and Euchner[28] recently found that even a slight increase of the bubble point pressure above atmospheric (15–20 bar) lowered the precipitation temperature by about 5 °C. Experiments in our laboratory with oil no. 6 in this study indicated that a reduction of the bubble point pressure from 395 bar to ambient, brought about by differential liberation of gas, elevated the crystallization temperature from about 20 °C to about 40 °C. This was interpreted as enhanced solubility of the wax components in the presence of dissolved gas. Loss of high molecular weight paraffins, caused by too low temperatures during surface sampling or surface transfer of bottom-hole samples, may also cause a depression of the WPT. For meaningful and reproducible WPTs (and rheological data) to be obtained, this source of error and uncertainty has to be minimized by sampling and transfer at sufficiently high temperature and careful treatment of the samples in the laboratory.

Table VII. Wax Dissolution Temperatures (WDT) of the Oils Investigated, Determined by Microscopy and DSC[a]

oil no.	WDT from microscopy	ΔT[b]	WDT from DSC	ΔT[b]
1	50	19	37.0	27.0
2	51	12	30.5	13.5
3	53	12	40.0	6.5
4	55	7	46.5	14.0
5	50	10	53.5	14.0
6	53	14	46.5	7.0
7	53	18	47.0	15.0
8	51	13	53.0	21.0
9	46	10	48.5	17.0
10	42	1	40.0	8.5
11	50	28	34.0	c
12	38	6	37.5	12.0
13	nd		-16.0	10.0
14	41	7	40.5	17.5
15	50	15	35.5	15.0
16	37	0	43.5	9.5
17	42	3	39.0	15.0

[a] Heating and cooling rates 10 °C/min. [b] Difference between dissolution temperature on heating and crystallization temperature on cooling (WDT – WPT). [c] WPT could not be determined.

Wax Dissolution Temperatures. Ideally, under equilibrium conditions, the crystallization of wax on cooling and dissolution on heating should occur at the same temperature. However, in general, when crystallization and dissolution is studied experimentally, "practical" cooling and heating rates prevent perfect thermal equilibrium. Thus, observed crystallization and dissolution temperatures are likely to be lower and higher, respectively, than those predicted from pure solubility equilibrium considerations. This will show up as an *apparent* hysteresis. It can, however, in principle be avoided by cooling and heating slowly enough. Perhaps more important is the fact that a nucleation process with a certain activation energy inevitably is involved in the crystallization, the physical expression of which is a certain degree of supersaturation and hence supercooling.[55] The combined effect of these two factors was examined in the microscope (cooling and heating rate 0.5 °C/min) and by the DSC method (cooling and heating rates 10 °C/min) by reheating the samples from room temperature and −145 °C, respectively, to beyond the dissolution temperatures (WDT). The results are summarized in Table VII. In some cases it was rather difficult to determine the dissolution temperature accurately in the microscope. The DSC data were therefore thought to be most reliable for the purpose of quantifying the effect, although this method also suffered from un-

(55) Walton, A. G. *Science* **1965**, *148*, 601–607.

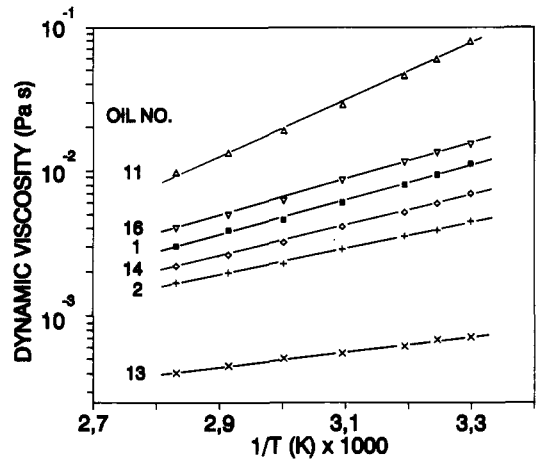

Figure 8. Typical Arrhenius plots of the Newtonian viscosities of some oils in the temperature range from 80 to 30 °C. The viscosity data are seen to be well fitted to the Arrhenius equation (eq 2). The slopes of the curves are equal to E_a/R. The aromatic/naphthenic biodegraded oils no. 1 and 11 and the asphaltene-rich oil no. 16 are seen to be most viscous and also to have the highest activation energies. See Table VIII.

certainties due to difficulties in defining an appropriate processing baseline in some cases. However, both methods showed the same trend; in each case the melting/dissolution endotherm was shifted to higher temperatures than the crystallization exotherm. The large ΔT (WDT − WPT), 27 °C, for oil no. 1 is considered particularly uncertain. But, for the other oils, ΔT varied between 6 and 20 °C, on average about 14 °C, which is slightly more than observed by Noel for lubricating oils.[50] As discussed above, only a negligible difference could be attributed to nonequilibrium due to high scan rates. Hence, a substantial supercooling obviously occurred in these complex wax–oil solutions.

This phenomenon may have implications with respect to wax deposition. First, precipitates and deposits already formed will require a higher temperature to redissolve. Second, if an oil is somehow reheated from below the crystallization temperature, deposition may continue to take place even at a higher temperature.

Activation Energies of Viscous Flow. As pointed out above, at temperatures in excess of 30–40 °C, crude oils generally behave Newtonian, no matter whether the oil is waxy or not. The Newtonian viscosity is essentially determined by the hydrocarbon group type distribution (alkanes, cycloalkanes, aromatics, resins, asphaltenes) and the carbon number distribution. As a rule, crude oils rich in condensed aromatics (such as oils no. 1 and 11) and asphaltenes (such as oil no. 16) will have the highest Newtonian viscosities. Moreover, the higher the average carbon number, or roughly the average molecular weight, the higher is the viscosity, partly because of lower content of low molecular weight paraffin solvents and partly because the heavy end has a higher proportion of condensed aromatics and particularly asphaltenes. It can be noted in Table II that the highly bidegraded, almost wax-free oil no. 11 in fact had viscosities comparable to the waxy oils even at low temperatures. This clearly illustrates the strong effect of high molecular weight aromatics and naphthenes on the viscosity of an oil.

Figure 8 shows some typical Arrhenius plots of Newtonian viscosities at temperatures higher than 30 °C. As can be inferred from the linearity of the curves, the Newtonian viscosity of a crude oil is uniquely defined over a broad temperature range in terms of two experimental constants, namely the constant A and the activation energy E_a in the Arrhenius equation (eq 2). By linearizing the exponential equation, it is easily seen that E_a is given by

$$E_a = R\ \mathrm{d}(\ln \mu)/\mathrm{d}(1/T) \tag{3a}$$

or

$$E_a = 2.303R\ \mathrm{d}(\log \mu)/\mathrm{d}(1/T) \tag{3b}$$

The slopes of the curves in Figure 8 are thus equal to E_a/R. The activation energies obtained by linear regression of $\log \mu$ against $1/T$ are summarized in Table VIII. For most of the "normal" paraffinic oils, the activation energies are seen to be fairly constant around 20 kJ mol^{-1}. The general trend was that the heaviest oils, and the highly biodegraded oil no. 11 (E_a = 37.4 kJ mol^{-1}) in particular, had the highest values of E_a, while the light oils and condensates had values on the order of 15 kJ mol^{-1} and lower, the light condensate no. 13 as low as 10 kJ mol^{-1}. This value is somewhat higher than E_a values calculated from viscosity–temperature data of some pure n-alkanes, published by Knapstad et al.[56] and Reid et al.[57] (see Table IX). For instance, for n-C_{32} and n-C_{44}, E_a values of 8.33 and 9.26 kJ mol^{-1} respectively were calculated. Condensate no. 13 contained less than 2 wt % of C_{20+} material and had an

Table VIII. Activation Energies of Newtonian Flow E_a and Regression Constants in the Linearized Arrhenius Equations of Oils Investigated[a]

oil no.	E_a, kJ mol^{-1}	log A	RSD,[b] %	R^2[c]
1	23.0	−5.92	3.2	0.997
2	17.5	−5.37	2.3	0.997
3	20.5	−5.68	4.7	0.991
4	15.0	−5.25	2.1	0.997
5	21.1	−5.62	1.6	0.999
6	20.4	−5.66	2.5	0.996
7	21.1	−5.85	8.4	0.983
8	18.1	−5.45	2.2	0.998
9	23.8	−6.05	3.7	0.996
10	14.4	−5.12	2.1	0.996
11	37.4	−7.56	4.6	0.997
12	14.8	−5.28	4.0	0.990
13	10.2	−4.89	1.4	0.998
14	20.6	−5.71	2.0	0.998
15	14.6	−5.21	2.4	0.995
16	24.3	−5.99	2.4	0.998
17	21.8	−5.90	6.2	0.986

[a] Regression equation: $\log \mu = a + b(1/T)$, where $a = \log A$ and $b = E_a/R$, $R = 8.31 \times 10^{-3}$ kJ mol^{-1} K^{-1}. [b] Relative standard error in the viscosity estimate. [c] Correlation coefficient squared.

Table IX. Activation Energies of Newtonian Flow for Some Pure Hydrocarbons[a]

compd	temp interval, °C	E_a, kJ mol^{-1}	RSD,[b] %	R^2[c]	ref
n-C_7	−40 to 100	3.42	0.7	0.9999	57
n-C_{10}	20 to 80	4.55	0.4	0.9999	56
n-C_{12}	20 to 80	5.32	0.9	0.9996	56
n-C_{14}	20 to 80	6.11	1.2	0.9994	56
n-C_{32}[d]	80 to 152	8.32	1.4	0.9994	56
n-C_{44}[d]	96 to 175	9.26	2.7	0.9983	56
toluene	−20 to 110	3.92	0.8	0.9999	57
m-xylene	0 to 140	3.81	0.7	0.9999	57

[a] Calculated using viscosity–temperature data from the specified reference. [b] Relative standard error in the viscosity estimate. [c] Correlation coefficient squared. [d] Viscosities measured at 3 bar pressure. The other viscosities were measured at atmospheric pressure.

(56) Knapstad, B.; Skjølsvik, P. A.; Øye, H. A. *J. Chem. Eng. Data* 1987, *34*, 37–43.
(57) Reid, R. C.; Prausnitz, J. M.; Sherwood, T. K. *Properties of Gases and Liquids*, 3rd ed.; McGraw-Hill Inc.: New York, 1977; pp 450–452.

average carbon number around C_{10}. Thus, the presence of branched alkanes, naphthenes, and aromatics obviously had the effect of increasing E_a as compared to pure *n*-alkanes. This also explains the higher activation energies of the heavier oils which contain large polyaromatic and naphthenoaromatic molecules (extending to asphaltenes with very high molecular weights) as well as long, branched alkane chains. It is reasonable to believe that higher energy barriers then have to be overcome for flow to occur, due to stronger molecular interactions. Khong et al.[58] measured flow activation energies on the order of 150 kJ mol^{-1} for asphaltic material, which might be viewed as a kind of extremely heavy oil. The increasing flow activation energy with increasing content of high molecular weight material is illustrated in Figure 8 by the larger slopes for oils no. 1, 16, and 11.

Often, second- and higher-order ($1/T$) terms are included in the Arrhenius equation[56] to achieve better fit. However, as seen in Table VIII, use of the simple Arrhenius equation sufficed to achieve relative standard deviations in the viscosity estimates generally better than 5% and correlation coefficients typically on the order of 0.997. A possible source of error which would tend to increase the viscosity at high temperature and hence lower the calculated flow activation energy is loss of volatile components from the viscometer tube. This error is, however, believed to be very small due to the almost negligible surface area exposed to air, and moreover, much effort was spent on minimizing it. Another source of error is the densities at high temperature which were used to convert kinematic viscosities to dynamic viscosities. The table used to extrapolate from 15 °C (API 2540) assumes a standard thermal expansion coefficient for oils. In practice, it is likely to depend somewhat on composition, and in particular on volatile components. However, for some oils studied, densities at 50 °C calculated from measured densities at 15 °C have been found to agree with measured densities within 0.5%, generally on the low side. It thus appeared that the crude oils studied had a slightly larger expansion coefficient than assumed in the API table, the effect being that calculated dynamic viscosities at the highest temperatures would be correspondingly underestimated. The errors in activation energy resulting from loss of volatile components and density extrapolation were therefore likely to more or less cancel out, the combined error probably being within the standard deviation in the regression line.

As seen in Figure 6b, the slopes of the log η against $1/T$ plots increased as waxes started to precipitate. A likely interpretation is that the *apparent* activation energy of flow increases. This is reasonable because the fluids eventually approach a solidlike or gelled state where the movement of individual molecules is highly restricted. However, these activation energies are at least not uniquely defined, as it is seen in Figure 6b that the slope varied considerably with shear rate, cooling rate, and thermal pretreatment. Even for a given set of conditions, the slope was generally seen to decrease with decreasing temperature. Because it is not quite clear whether the apparent activation energies of flow retain the full significance attached to the activation energy in Newtonian flow, we will not elaborate this subject any further at present.

Summary and Conclusions

Nearly all the oils studied were found to benefit from thermal pretreatment, i.e., preconditioning at 80 °C, in that the pour points and viscosities in the non-Newtonian temperature range (generally below 30 °C) were lowered. The pour points were in some cases lowered by as much as 30–40 °C. This reflects the action of inherent pour point depressants (asphaltenes, resins) present in the oils. The exceptions to this rule were the condensates, which hardly contain any inherent pour point depressants.

The pour point of thermally pretreated oil (minimum pour point) was in most cases 40–60 °C lower than the WPT. On average, about 4 wt % precipitated wax (pulsed NMR data) was present at the minimum pour point. At the non-Newtonian temperature limit about 1 wt % was found to be present.

Isoalkanes were the most abundant hydrocarbon class in wax filtered from one of the oils at 40, 23, and 6 °C. The ratio isoalkanes/*n*-alkanes was increasing with decreasing filtration temperature. The peak in the *n*-alkane distribution shifted from C_{50} to C_{42} and C_{33} for the 40, 23, and 6 °C waxes, respectively. There were clear indications that the relative amount of polycyclic naphthenes was higher near the crystallization temperature than at lower temperatures.

In polarization microscopy, the observed WPTs were found to be about 3 °C lower at cooling rate 0.5 °C/min than at 0.1 °C/min and to get lower with increasing film thickness (in the range from about 10 to about 150 μm). Standard conditions adopted were 0.5 °C/min and approximately 50 μm film thickness. In the DSC measurements, only a negligible effect of scan rate on crystallization temperatures was observed. With the exception of the most waxy oils, WPTs determined by microscopy were in general about 10 °C higher than DSC and viscometry values. WPTs from microscopy probably are the most relevant for predicting initial onset of wax *deposition* in production equipment, flow lines etc. Transition from Newtonian to non-Newtonian rheological behavior generally occurred a few degrees below the DSC and viscometric WPTs.

Wax dissolution temperatures were on average about 14 °C higher than the corresponding crystallization temperatures. This indicated that substantial supercooling was taking place in the oils.

The dynamic viscosity in the Newtonian temperature range of the oils (i.e., generally above 30 °C) generally obeyed a simple first-order Arrhenius type of temperature dependence: $\mu = A \exp(E_a/RT)$. Relative standard errors in the viscosity estimates were in general less than 5% and correlation coefficients about 0.997. The calculated activation energies of Newtonian viscous flow were in most cases around 20 kJ mol^{-1}, while for the light oils and condensates they were 10–15 kJ mol^{-1} and for the heavy, biodegraded oils up to 37 kJ mol^{-1}. Activation energies of flow in the non-Newtonian temperature range are not uniquely defined.

Acknowledgment. We gratefully acknowledge the experimental assistance by Liv Aa. Tau and Ingun Skjevrak (GC/MS), both Statoil, and Anne B. Nielsen, Risø. We also are grateful to Statoil for permission to publish this paper.

Abbreviations

DSC	differential scanning calorimetry
HTGC/MS	high-temperature gas chromatography/mass spectrometry
NMR	nuclear magnetic resonance
PPD	pour point depressant
WDT	wax dissolution temperature

(58) Khong, T. D.; Malhotra, S. L.; Blanchard, L.-P. *Inst. Pet. Technol.* **1978**, paper IP 78-001.

WPT wax precipitation temperature

Nomenclature

A	constant in Arrhenius equation
a	linear regression constant
b	linear regression coefficient
E_a	activation energy of viscous flow, J mol^{-1}
R	gas constant (=8.3144 J K^{-1} mol^{-1})
T	temperature, K
T_g	glass transition temperature, K
η	apparent (shear rate dependent) viscosity, Pa s
μ	dynamic viscosity, Pa s
ν	kinematic viscosity, cSt (=10^{-2} mm^2 s^{-1})
ρ	mass density, kg m^{-3}

Wax Precipitation from North Sea Crude Oils. 2. Solid-Phase Content as Function of Temperature Determined by Pulsed NMR

Walther B. Pedersen,* Asger B. Hansen, Elfinn Larsen, and Anne B. Nielsen

Risø National Laboratory, DK-4000 Roskilde, Denmark

Hans Petter Rønningsen

STATOIL a.s., Forus, N-4001 Stavanger, Norway

Received April 29, 1991. Revised Manuscript Received September 9, 1991

A simple, low-resolution pulsed NMR method was applied for determining the amount of solid phase at different temperatures in 17 crude oils of different origins. Protons present in the oils were excited by a pulse of radio frequency radiation. After the pulse, the decay in magnetization was characterized by its signal amplitude obtained 10 and 70 μs after the pulse. The first signal was proportional to the number of protons in the solid and liquid phases, and the latter signal was proportional to the number of protons in the liquid phase. The NMR signals were calibrated against samples of polyethylene dispersed in a wax-free oil. For most of the oils investigated, except for some biodegraded and asphaltenic oils, the NMR estimated solid-phase content at −40 °C correlated well with the amount of wax determined by acetone precipitation at −25 °C. This pulsed NMR method was demonstrated to be capable of determining the temperature dependence of the solid-phase content of crude oils during a *single* working day.

Introduction

Wax precipitation temperatures and the amount of wax precipitated at a given temperature are important characteristics of crude oils as discussed in part 1 of this series of papers.[1-3] Experimental data on wax precipitation are normally limited to determining the cloud point temperature and total wax content of each oil. A detailed characterization of the wax content as function of temperature is very important for establishing thermodynamic models of wax formation in crude oils with good predictive capability. The correct measurement of the amount of solid wax in partially frozen oils, especially black oils, by filtration is not easy due to considerable contribution from entrapped oil.[4] The same problem applies to centrifugation. The objective of this work was by some alternative method to provide reasonably accurate solid content vs temperature data required for the estimation of various parameters in the thermodynamic model described in part 4[3] of this series of papers. The present paper describes the determination of the solid content of crude oils at different temperatures using a low-resolution pulsed nuclear magnetic resonance (NMR) technique.

NMR is well documented as a powerful technique for chemical analysis, whereas its use for characterizing physical properties and distinguishing among different phases of crude oils is rare.[5] However, pulsed NMR is used routinely in the food industry to determine the solid content in fats of different origins and develop new fat

Table I. Brief Description of Crude Oil Samples Studied in This Work

oil no.	description
1	biodegraded, aromatic oil
2	paraffinic oil
3	waxy oil
4	waxy condensate
5	waxy oil
6	waxy oil
7	paraffinic oil
8	paraffinic oil
9	waxy oil
10	light, paraffinic oil
11	heavy, biodegraded, naphthenic oil
12	paraffinic condensate
13	very light, paraffinic condensate
14	waxy oil
15	paraffinic oil
16	paraffinic, asphaltenic oil
17	paraffinic oil

* To whom correspondence should be addressed.

(1) Rønningsen, H. P.; Bjørndal, B.; Hansen, A. B.; Pedersen, W. B. *Energy Fuels*, this issue.
(2) Hansen, A. B.; Larsen, E.; Pedersen, W. B.; Nielsen, A. B.; Rønningsen, H. P. *Energy Fuels*, this issue.
(3) Pedersen, K. S.; Skovborg, P.; Rønningsen, H. P. *Energy Fuels*, this issue.
(4) Van Winkle, T. L.; Affens, W. A.; Beal, E. J.; Mushrush, G. W.; Hazlett, R. N.; DeGuzman, J. *Fuel* 1987, *66*, 890-896.

0887-0624/91/2505-0908$02.50/0